Advances in Thermal Modeling of Laser Chemical Vapor Deposition and Infiltration

Yuwen Zhang
Department of Mechanical and Aerospace Engineering
University of Missouri
Columbia, MO 65211, USA

Table of Contents

ABSTRACT

Laser chemical vapor deposition and deposition (LCVD and LCVI) are based on the concept of building functional structures by deposition of solid materials from gas precursors by a laser beam in an environmentally controlled chamber. The chemical vapor deposition during these two processes can be based on reactions initiated pyrolytically, photolytically or a combination of both. The most important issue that the thermodynamic analysis can address is whether a given chemical reaction is feasible. For chemical reactions that are feasible, both composition plot and deposition maps can be obtained. The distinction between the conventional Chemical Vapor Deposition (CVD) and LCVD is that laser beam heats a very small spot on the substrate and vapor deposition occurs only in the heated spot in the LCVD process. A series of thermal models of LCVD of Titanium Nitride on a finite slab under irradiation by a moving laser beam have been developed. Heat transfer in the substrate and gases, the chemical reaction on

the substrate's top surface, and the mass transfer of gases in the chamber were taken into account. The effect of natural convection induced by the temperature and concentration gradients during LCVD was instigated. A parametric study on the LCVD by moving laser beam was carried out and an empirical correlation was proposed. To study the transport phenomena in LCVI, heat transfer in a gas-saturated powder layer subject to a short-pulsed volumetric heat source is modeled using a two-temperature model. The results show that the non-equilibrium is significant when the heat source pulse width is less than 1 microsecond and therefore, heat transfer during nanosecond laser- powder interaction should be modeled using non-equilibrium model. For the case with long pulse width, on the other hand, the equilibrium model is sufficient.

1. INTRODUCTION

Gas-phase Solid Freeform Fabrication (SFF), which includes Laser Chemical Vapor Deposition (LCVD) and Laser Chemical Vapor Infiltration (LCVI), is an emerging manufacturing technology of in which three-dimensional parts can be built from CAD data. The gas-phase SFF process consists of two steps (Marcus *et al.,* 1993): (1) design a three-dimensional part with CAD and the CAD data is then transferred to a STL computer file, which is sliced to generate two-dimensional sections of the *virtual product,* (2) build the *physical product* by layering two-dimensional sections of finite thickness.

An extremely wide array of SFF technologies has been proposed for purposes of providing physical three-dimensional renderings of CAD data. However, only a few have been extended to build *structurally-sound* parts of near full density. Almost always, the SFF technologies that fit into the latter group are powered by *thermal fabrication* of three-dimensional objects from powders or gases. The heat source is nearly always a laser operating in infrared regions of the electromagnetic spectrum. To produce fully functional structural components, gas-phase SFF (such as LCVD and LCVI), seems to be very promising. The distinctive advantage of gas-phase SFF over other SFF techniques is that the local chemical compositions of the final product can be tailored by the control of the composition of precursors, deposition temperature and wavelength of the laser beam.

LCVD/LCVI are based on the concept of building functional structures by deposition of solid materials from gas precursors by a laser beam in an environmentally controlled chamber. The chemical vapor deposition during these two processes can be based on reactions initiated pyrolytically, photolytically or a combination of both (Marcus *et al.,* 1993). The LCVD technique uses precursors to directly create free-standing part or to join together simple shapes to create parts with higher complexity [see Fig. 1(a)]. On the other hand, LCVI uses gas precursors *and* powder particles to build three-dimensional parts [see Fig. 1(b)], which is similar to other powder-based SFF techniques, such as Selective Laser Sintering (SLS). The advantages of LCVI over LCVD include (a) uninfiltrated powder provides support for producing overhangs, (b) confining the deposition to thin powder layers provide dimensional control in the direction of growth, and (c) it is possible to tailor local chemistry and microstructures (Jakubenas *et al.*, 1997).

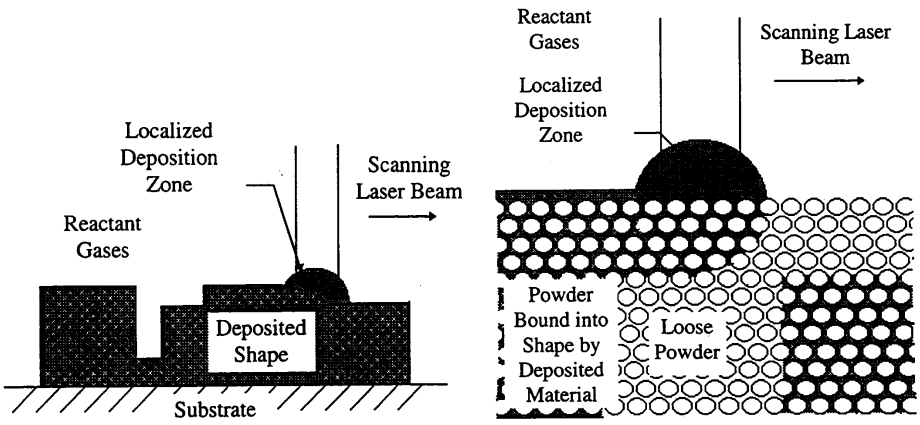

(a) LCVD (b) LCVI

Figure 1 Schematic of SALD and SALDVI (Jakubenas *et al.,* 1997).

The chemical reactions in LCVD and LCVI are same as those occurring in the conventional Chemical Vapor Deposition (CVD; Mahajan, 1996), which is widely used to fabricate semiconductor devises. It depends on availability of a volatile gaseous chemical that can be converted to solid film through some thermally activated chemical reaction. The CVD can be used to produce a large variety of thin films with different precursors. It is very crucial that the chemical reaction takes place on the substrate surface only, so that a thin film can be deposited onto the substrate. If undesired chemical reactions occur in the gas phase, the solid particles can be formed which may fall onto the substrate or coat the chamber walls. To avoid the undesired chemical reaction, the substrate surface temperature, deposition time, pressure, and surface specificity should be carefully selected. The chemical reaction during a CVD process is usually accomplished in several steps and the path of chemical reactions can be altered by changing the substrate temperature. For example, when titanium tetrabromide ($TiBr_4$) is used as a precursor to deposit titanium film, the chemical reaction is accomplished in the following steps (Mazumder and Kar, 1995):

$$TiBr_4(g) \rightarrow TiBr_2(s)+Br_2(g)$$

$$3TiBr_2(s) \rightarrow 2TiBr(s)+TiBr_4(g)$$

$$4TiBr(g) \rightarrow 3Ti(s)+TiBr_4(g)$$

The mechanisms of chemical reactions for many CVD processes are not clear, so the chemical reactions occurring in a CVD process are often represented by a single overall chemical reaction equation. Table 1 summarizes some examples of the overall chemical reactions occurring in CVD processes (including LCVD and LCVI).

Figure 2 shows a reaction chamber for a LCVD process (Marcus *et al.*, 1993). In contrast to conventional CVD, in which the entire susceptor is heated, only a very small spot on the substrate is heated by a directed laser beam. Scanning of the substrate surface is accomplished by a movable table. After the first layer of the solid is deposited, consecutive layers can be deposited to build the three-dimensional part based on the CAD design. The pressure inside the chamber is usually under 1 atm and the temperature of the spot under laser irradiation can

range from 700 to 1500 °C. Successful deposition of various ceramic and metallic materials using various gaseous precursors has been reported.

Table 1 Overall chemical reaction of CVD processes

Thin films	Overall reaction	Temperature of reaction	References
Al_2O_3	$Al(l) + H_2O(g) = AlO(g) + H_2(g)$ $AlO(g) + H_2O(g) = Al_2O_3(s) + H_2(g)$	1230-1255°C	Powell *et al.* (1966)
C	$C_xH_y(g)=xC(s)+(y/2)H_2(g)$	700-1450°C	Taylor *et al.* (2004)
GaAs	$GaCI(g) + (1/4)As4(g) = GaAs(s) + HCI(g)$		Sivaram (1995)
GaAs	$GaAs(g) + HCI(g)$ $=GaCI(g) + 1/4(As_4(g)) + 1/2(H_2(g))$	700-850°C	Sivaram (1995)
	$Ga(CH_3)_3+AsH_3 = GaAs+3CH_4$ $Al(CH_3)_3+AsH_3 = AlAs+3CH$	500-800°C	Ueda (1996)
GaN	$Ga(g) + NH_3 = GaN(s) + (3/2)H_2(g)$	650°C	Elyukhin *et al.* (2002)
Ge(s)	$GeH_4 =Ge(s) + 2H_2$		Herring (1990)
Si	$SiH_4(g)=Si(s)+2H_2(g)$	>600°C (polysilicon) >850-900°C (single crystal)	Herring (1990)
SiC	$Si(CH_3)_4(g)=SiC(s)+3CH_4(g)$	700-1450 °C	Sun *et al.* (1998b)
SiO_2	$SiH_4+ O_2 = SiO_2 + 2H_2$		Sivaram (1995)
	$SiH_4 + 2N_2O = SiO_2 + 2H_2O + 2N_2$	800°C	Sivaram (1995)
	$SiH_2Cl_2 + 2N_2O = SiO_2 + 2HCI + 2N_2$	> 900°C	Sivaram (1995)
TiO_2	$TiCl_4(g)+O_2(g)=TiO_2(S)+2Cl_2(g)$		Jakubenas *et al.* (1997)
TiN	$TiCl_4(g)+2H_2(g)+(1/2)N_2(g)=TiN(s)+4HCl(g)$	900°C	Mazumder and Kar (1995)

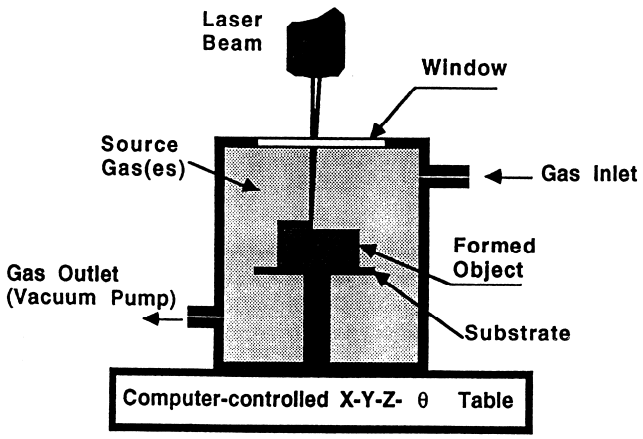

Figure 2 LCVD system (Marcus et al., 1993).

Figure 3 shows a schematic diagram of a LCVI system. The mechanism to bound powder particles together in a LCVI process is deposition of solid material on the powder particle surface by decomposition of gas precursors. During the LCVI process, a thin (100 - 250 μm thick) powder layer is laser-scanned to form the two-dimensional slice to an underlying solid piece, which consists of a series

of stacked two-dimensional slices. After laser scanning, a fresh powder layer is spread and the scanning process is repeated. Loose powder is removed after the part is extracted from its bin. The finished part has a composite structure that consisting of starting powder bonded into a matrix of the deposited materials (Birmingham and Marcus, 1994).

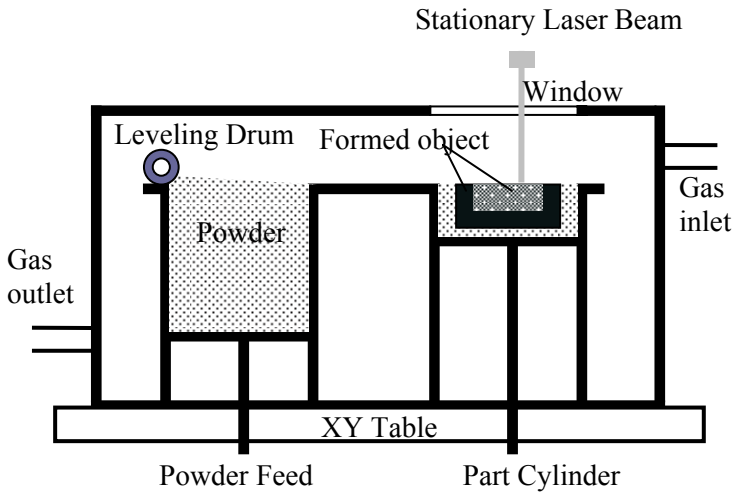

Figure 3 LCVI system (Zhang, 2006).

Extensive experimental works on LCVD/LCVI have been carried out and various applications of these new techniques have been discovered. The inherent nature of LCVD/LCVI makes them very ideal to fabricate ceramics and metal parts that are either impossible or very difficult to be manufactured by any other methods. Another advantage of LCVD/LCVI is that the composite of the parts can be varied by variation of several easily controlled process parameters, such as composition of gas precursors and the local deposition temperature. Sun *et al.* (1998a, b, c) fabricated *in situ* thermocouples into macro-components using combined LCVD and LCVI techniques. The bulk shape was built by using LCVI and the SiC/C thermocouples were deposited using LCVD technique. Two layers of Si_3N_4 were deposited below and above the SiC/C thermocouples so that the thermocouple legs are electronically insulated from the bulk shape into which the thermocouples is embedded. Crocker *et al.* (1998) embedded multiple SiC/C thermocouples in the SiC bulk shape using LCVD technique. Crocker *et al.* (2000; 2001; 2002) presented LCVI of SiC into metal and ceramic powders to fabricate composite parts.

Jean *et al.* (1999) designed a LCVD system with a fixed 100 W CO_2 laser focused on a movable substrate. Temperatures and height were monitored to provide feedback for controlling the process. Jean *et al.* (2000) studied precision carbon deposition using the LCVD system described in Jean *et al.* (1999) and found that the carbon deposit grew uncontrollably if constant laser power was used. LCVD can also find its application in micro manufacturing. Deposition of

rods, fibers, coils, and blocks as well as other complicated structures (such as microcoils) with different metal and ceramic materials have been achieved (Maxwell *et al.,* 1997). Maxwell *et al.* (1998a) successfully fabricated high field density microsolenoids from 100 to 500 μm in diameter using 3-D LCVD technique. Two different ways in which 3D-LCVD can be used to generate a microcoil are investigated: (a) direct–writing of a conductive line on an insulated fiber, or (b) freeform growth (Fig. 4). Maxwell *et al.* (1999) and William *et al.* (1999) deposited carbon in the form of helical spring and the fiber diameter of the spring was as small as 5 μm and the spring inner diameter was as small as 60 μm. Maxwell *et al.* (1998b) deposited high-aspect-ratio Titanium Nitride needles up to 12 mm long using $Ti(N(CH_3)_2)_4$ as precursor.

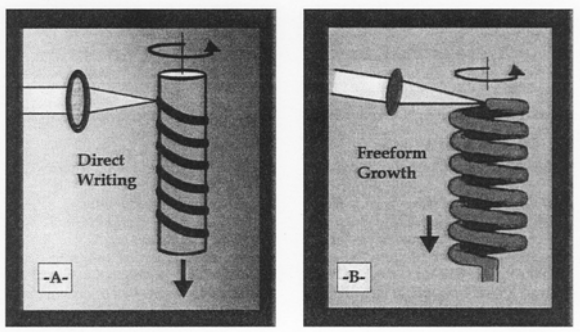

Figure 4 Techniques for growing coils using 3D-LCVD (Maxwell *et al.,* 1998a)

2. ADVANCES IN LCVD/LCVI RESEARCH

2.1 Thermodynamics and Kinetics of Chemical Reactions

Accurate prediction and control LCVD/LCVI require a model of the processes that incorporate heat/mass transfer, chemical reaction kinetics, and chemical thermodynamics. Kinetic data that are important to modeling LCVD/LCVI are difficult to obtain and are currently compiled for only a limited number of chemical systems. Realizing these difficulties, Jakubenas *et al.* (1997, 1998) presented thermodynamic modeling of LCVD/LCVI for various precursors using a computer code CET89 based on minimization of system free energy (Gordon and McBride, 1976). Sun *et al.* (1998a) performed thermodynamic analysis using the same code for *in-situ* thermocouples in macro-components fabricated using LCVD and LCVI techniques. The gaseous precursors considered include tetramethylsilane (TMS) and methyltrichlorosilane (MTS) for deposition of SiC, and methane, ethylene, and acetylene for deposition of carbon. The most important issue that the thermodynamic analysis can address is whether a given chemical reaction is feasible. For chemical reactions that are feasible, both *composition plot* and *deposition maps* can be obtained (Jakubenas *et al.*, 1998). The composition plot shows the equilibrium composition vs. a process parameter, such as temperature (see Fig. 5). Deposition maps, on the other hand, show only the equilibrium solid phase exists as fields in the plane defined by temperature and the initial reactant mixture (see Fig. 6). Thermodynamic modeling is very

useful for precursor selection; however, it *cannot* predict the deposition rate that is very critical for design of LCVD/LCVI systems.

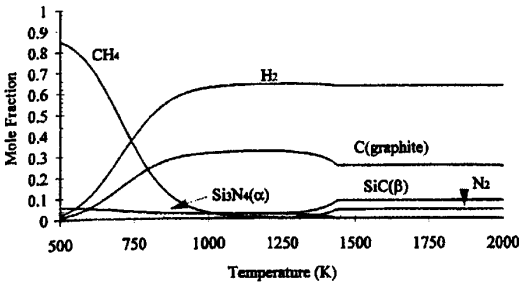

Figure 5 Composition vs. temperature for a 1:1 mixture of TMS and NH_3 at 0.5 atm and at thermodynamic equilibrium (Jakubenas et al., 1998)

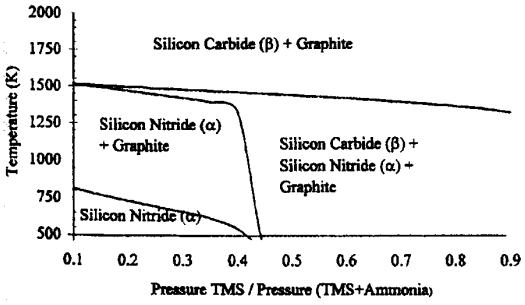

Figure 6 Deposition map for mixture of TMS and NH3 at 0.5 atm and at thermodynamic equilibrium (Jakubenas et al., 1998)

In order to accurately predict the reaction rate and the composition in the final product, the knowledge of chemical reaction and heat and mass transfer is needed. The kinetic equation, which express deposit rate as function of surface temperature and concentration, serves as constitutive relation in modeling of LCVD/LCVI process. For the deposition of TiN film using $TiCl_4$, N_2 and H_2 as precursors (Conde *et al.*, 1992a; Zhang and Faghri, 2000), the deposit rate $d\delta/dt$ was obtained by:

$$\frac{d\delta}{dt} = \frac{K_0}{\rho_{TIN}} \exp\left(-\frac{E}{R_u T_s}\right) C_s \tag{1}$$

where $K_0 = (C_{H_2})_i (C_{N_2})_i^{1/2} K_0^{'}$ and K_0' is Arrhenius constant, ρ_{TiN} is the density TiN, E is the activation energy, R_u is the universal gas constant, T_s is the local surface temperature, and C_s represents the concentration of $TiCl_4$ at the surface of the substrate. For deposition of SiC with $Si(CH_3)_4$ as precursor gas, a similar kinetic equation was employed by Lee *et al.* (1995). In order to incorporate the kinetic equation into the model of LCVD/LCVI, both Arrhenius constant K_0' and activation energy E must be determined. For conventional chemical vapor deposition of SiC using TMS as precursor and N_2 as carrier gas, Figueras *et al.* (1991a,b; 1992) obtained the apparent activation energy of 90 kJ/mol. Conde *et al.* (1992b) developed an analytical model and determined the values of these two constants that best matched the analytical and experimental results. For deposition of SiC with $Si(CH_3)_4$ as precursor gas, Lee *et al.* (1995) determined Arrhenius constant by fitting experimental data. In order to develop global models for LCVD/LCVI, Arrhenius constant and the activation energy must be obtained.

2.2 Thermal Modeling of LCVD Processes

The distinction between the conventional Chemical Vapor Deposition and LCVD is that laser beam heats a very small spot on the substrate and vapor deposition occurs only in the heated spot in the LCVD process. Kar and Mazumder (1989) presented a 3-D transient thermal analysis for LCVD on a

uniformly moving slab, in which a 3-D, non-linear, transient conduction problem was solved analytically. Kar *et al.* (1991) investigated laser chemical vapor deposition of Titanium on stationary finite slabs by solving 3-D, transient mass diffusion equations. Conde *et al.* (1992a) presented a model of laser chemical vapor deposition of Titanium Nitride (TiN) dots produced by the following overall chemical reaction: $TiCl_4(g) + 2H_2(g) + \frac{1}{2}N_2(g) \rightarrow TiN(s) + 4HCl(g)$. The 3-D transient diffusive mass transfer equation was solved using Fourier's transformation method. The volcano-like profile of the deposited film is found in certain conditions, which was in good agreement with the experimental data (Conde *et al.,* 1992b). Conde *et al.* (1992a), however, did not consider the heat transfer of the gases in the chamber.

Marcus *et al.* (1993) studied the residual stresses in laser processed SFF that included LCVD. Heat conduction in the substrate was modeled as a pure conduction problem with a moving heat source. Jacquot *et al.* (1995) proposed a thermal model of the LCVD process using acetylene (C_2H_2) as precursor. Various phenomena, which included heat conduction in the substrate, chemical reaction during carbon deposition and mass diffusion of acetylene in the chamber, were taken into account. The temperature of the gases is assumed to be uniform and therefore the heat transfer in the gas phase was neglected. Shaarawi *et al.,* (2000) presented a 2-D axisymmetric model of LCVD of SiC rods from tetramethylsilane (TMS), which included heat and mass transfer and chemical reaction in the model. Zhang and Faghri (2000) developed a very detailed model of LCVD process, which included the submodels of heat transfer, chemical reaction and mass transfer, and the model was employed to simulate the laser chemical vapor deposition of TiN film on a finite slab with stationary and moving laser beams. The above efforts assumed that the deposited film was very thin and heat transfer in the thin film was not taken into account, which was valid only for the first layer of deposition. In order to build 3-D part, multiple layer deposition will be needed and heat conduction in the continuously growing part needs to be accounted for in the model. This is especially the case when depositing layer and the substrate has significantly different thermal conductivity (Han and Jensen, 1994). To obtain the surface temperature that is critical to predict the growth rate [see eq. (1)], the heat transfer model must be able to account for the effect of part growth on the temperature distribution.

2.3 Thermal Modeling of LCVI

The physical and chemical phenomena occurred in LCVI are similar to that in LCVD. The only difference is that vapor deposition occurs on the surface of the powder particles during LCVI, instead of on the top of non-porous substrate in LCVD. Laser processing in LCVI is complicated by the fact that the irradiated material responds differently than in the case for a simple, fully dense material. Successful modeling of the LCVI process also requires knowledge about kinetics

of chemical reaction, fluid flow, and heat and mass transfer in the precursors and in the porous powder bed. In addition, radiation heat transfer in powder bed also plays an important role in the heat transfer analysis due to the high temperature involved. Convective heat transfer in porous media has been extensively investigated in the past and very detailed reviews are available in the literature (Nield and Bejan, 1999; Kaviany, 1995). The distinctive feature of heat transfer and fluid flow in the LCVI process is that the porosity is not constant. The chemical reaction that occurs on the surface of the particle results in deposition on the surface of the powder particles and eventually joins the powder particles together. During the entire process, the porosity may change from a large value, up to 0.6, to nearly zero.

Dai *et al.* (2000) performed numerical simulation of LCVI using a finite element commercial code ANSYS. The dependence of the powder bed properties on the porosity was taken into account. The powder bed before laser densification was assumed to be 50% of its theoretical density. The densities of the powder bed were set to 80% and 100% of its theoretical value when the temperature of the powder reached to 1200K and 1273K, respectively. This treatment directly correlated the density of the powder bed to the temperature and avoided the chemical reaction model. Dai *et al.* (2001) presented a finite element modeling of SALDVI with the same method and an experiment was also performed. In order to simulate the closed loop control used in the experiment, the laser power was modified from one time step to the next time step to ensure the powder bed temperature was a constant. The models of Dai *et al.* (2000, 2001) were improved later by incorporating a densification model by vapor infiltration based on experimental growth rate (Dai *et al.*, 2003). The effects of convection and mass transfer in the powder bed and precursors were not taking into account in any of the existing works. Compared to LCVD, the efforts on simulation of LCVI are extremely limited at this time.

3. PHYSICAL MODELS AND TRANSPORT PROPERTIES

3.1 Governing Equations

Since the velocity of the precursors is generally very low and the characteristic length is also very small, the corresponding Reynolds number is under 100 and the Grashof number governing natural convection is under 10^6. Therefore, the transport phenomena in the LCVD process are laminar in nature. The temperature in a reactor varies significantly (typically from 300 to 900K), so the Boussinesq approximation is no longer appropriate. It is necessary to use the compressible model for transport phenomena in LCVD processes. The following assumptions can be made to obtain the governing equations:

1. The only body force is the gravitational force, which is the same for all components in the precursors.
2. Dilute approximation is valid because the partial pressure of the reactant is much lower than that of the carrier gas.

3. The deposited film is very thin (from nanometers to microns) and its effect on the flow field can be neglected.

The continuity equation is

$$\frac{D\rho}{Dt} + \rho\nabla\cdot\mathbf{V} = 0 \tag{2}$$

where the precursor gases are treated as a compressible fluid mixture.

The momentum equation is

$$\rho\frac{D\mathbf{V}}{Dt} = \nabla\cdot\boldsymbol{\tau}' + \rho\mathbf{g} \tag{3}$$

where the stress tensor is

$$\boldsymbol{\tau}' = -p\mathbf{I} + 2\mu\mathbf{D} - \frac{2}{3}\mu(\nabla\cdot\mathbf{V})\mathbf{I} \tag{4}$$

The energy equation is

$$\rho c_p\frac{DT}{Dt} = \nabla\cdot(k\nabla T) + T\beta\frac{Dp}{Dt} \tag{5}$$

where the effect of viscous dissipation and the Dufour effect have been neglected.

For a system containing n_r reactants and n_p gaseous products, the chemical equation can be expressed as

$$\sum_{i=1}^{n_r} a_{ri}A_{ri}(g) = a_pA_p(s) + \sum_{i=1}^{n_p} a_{pi}A_{pi}(g) \tag{6}$$

where A_{ri} $(i = 1, 2\cdots n_r)$ are chemical symbols for the gaseous reactants, A_p and A_{pi} $(i = 1, 2\cdots n_p)$ are chemical symbols for the deposit (solid) and other gaseous products. The coefficients preceding the chemical symbols in eq. (6) are referred to as stoichiometric coefficients and describe the proportion of the mole numbers of reactants disappearing and mole number of products appearing as a result of the reaction process. The number of components in the precursors is $n = n_r + n_p$.

The conservation of species mass in terms of the mass fraction is

$$\rho\frac{D\omega_i}{Dt} = -\nabla\cdot\mathbf{J}_i + \dot{m}_i''', \quad i = 1, 2, \ldots N-1 \tag{7}$$

where ω_i is the mass fraction of the i^{th} component in the gaseous precursor. The mass flux $\mathbf{J}_i$ includes mass fluxes due to ordinary diffusion driven by the concentration gradient, and thermal (Soret) diffusion (Faghri and Zhang, 2006). The production rate of the i^{th} species, $\dot{m}_i'''$, can be obtained by analyzing the chemical reaction. If the number of chemical reactions taking place in the system is N_g, the mass production rate is (Mahajan, 1996)

$$\dot{m}_i''' = \sum_{j=1}^{N_g} a_{ij}^g M_i \Re_j^g \tag{8}$$

where a_{ij}^g is the stoichiometric coefficient for the i^{th} component in the j^{th} chemical reaction in the gas phase, and $\Re_j^g$ is the net reaction rate of the j^{th} chemical reaction in the gas phase (Faghri and Zhang, 2006).

The density of the gas is related to the pressure and temperature by the ideal gas law:

$$\rho = \frac{p}{R_g T} \tag{9}$$

The boundary conditions for the governing equations of a CVD process depend on the geometric configuration of the reactor. It is generally assumed that the nonslip condition is applicable to all solid walls. The normal velocity on a solid wall is zero (no penetration) for all walls except the susceptor where chemical reaction takes place. The total net mass flux of all species can lead to a normal velocity component on the susceptor as (Mahajan, 1996)

$$v_n = \frac{1}{\rho} \sum_{i=1}^{N} \sum_{j=1}^{N_s} a_{ij}^s M_i \Re_j^s \tag{10}$$

where a_{ij}^s is the stoichiometric coefficient for the i^{th} component in the j^{th} chemical reaction on the susceptor surface, and $\Re_j^g$ is the net reaction rate of the j^{th} chemical reaction on the susceptor surface.

The net surface reaction rate $\Re_j^g$ is a product of the sticking coefficient γ_j (fraction of product that can be stuck on the substrate) and the effusive flux of the j^{th} species (Mahajan, 1996), i.e.,

$$\Re_j^s = \gamma_j \frac{x_j p_j}{\sqrt{2\pi M_j RT}} \tag{11}$$

The growth rate of the deposit on the susceptor is

$$\frac{d\delta}{dt} = M_f \sum_{i=1}^{N} \sum_{j=1}^{N_s} a_{ij}^s \Re_j^s \alpha_{i,f} \tag{12}$$

where M_f is the molecular mass of the deposited film, and $\alpha_{i,f}$ is the number of film atoms in the i^{th} species.

3.2 Transport Properties

The thermophysical properties of various gaseous precursors are necessary to utilize the transport models outlined above. Since the temperature varies significantly throughout a CVD system, the transport phenomena must be modeled using variable thermal physical properties. This requires knowledge of the dependence of the thermophysical properties on temperature. The thermophysical properties of the commonly used gas(es) in CVD are tabulated in Table 3.

The viscosity and thermal conductivity of some precursors that are not readily available can be estimated using the method recommended by Bird *et al.* (2002). The viscosity is

$$\mu = 2.6693 \times 10^{-6} \frac{\sqrt{MT}}{\sigma^2 \Omega_\mu} \tag{13}$$

where M is the molecular mass and σ is the collision diameter (Å= 10^{-10} m) of the molecule that can be estimated by

$$\sigma = 0.841\bar{v}_c^{1/3} \tag{14}$$

or

$$\sigma = 1.166\bar{v}_{b,liq}^{1/3} \tag{15}$$

where $\bar{v}_c$ and $\bar{v}_{b,liq}$ are the specific volumes (cm^3/mol) of the precursor at critical point, and of the saturated liquid at normal boiling point, respectively.

Table 3 Transport properties of the common gas(es) for CVD (Mahajan, 1996)

Properties	Gas(es)	c_0	c_1	c_2
μ[a] (N-s/m²)	TMGa	-1.15×10^{-6}	3.35×10^{-8}	-6.68×10^{-12}
	AsH_3	-4.32×10^{-7}	5.94×10^{-8}	-1.46×10^{-11}
	H_2	2.63×10^{-6}	2.22×10^{-8}	-5.19×10^{-12}
	N_2	4.93×10^{-6}	4.55×10^{-8}	-1.08×10^{-11}
	SiH_4	1.47×10^{-6}	3.66×10^{-8}	-6.81×10^{-12}
k[a] (W/m-K)	TMGa	-3.52×10^{-3}	3.85×10^{-5}	-3.84×10^{-8}
	AsH_3	-7.16×10^{-3}	6.53×10^{-5}	-3.47×10^{-9}
	H_2	5.77×10^{-2}	4.43×10^{-4}	-7.54×10^{-8}
	N_2	8.15×10^{-3}	6.24×10^{-5}	-4.48×10^{-9}
	SiH_4	-2.12×10^{-2}	1.45×10^{-4}	-1.31×10^{-8}
c_p[a] (kJ/Kg-K)	TMGa	5.40×10^{2}	1.60	0
	AsH_3	2.45×10^{2}	1.08×10^{0}	-4.24×10^{-4}
	H_2	1.44×10^{4}	-2.61×10^{-1}	8.67×10^{-4}
	N_2	1.03×10^{3}	4.58×10^{-3}	1.34×10^{-4}
	SiH_4	4.74×10^{2}	3.26	-1.08×10^{-3}
D_{12}[b] (m^2/s)	SiH_4, N_2	-9.64×10^{-1}	6.25×10^{-3}	8.50×10^{-6}
	SiH_4, H_2	-2.90	2.06×10^{-2}	2.81×10^{-5}
	N_2, H_2	-3.20	2.44×10^{-2}	3.37×10^{-5}
	TMGa, H_2	-1.87	1.64×10^{-2}	3.13×10^{-5}
	TMGa, N_2	-4.17×10^{-1}	2.89×10^{-3}	4.93×10^{-6}
	AsH_3, H_2	-2.26	1.73×10^{-2}	2.80×10^{-5}
	AsH_3, N_2	-6.15×10^{-1}	4.57×10^{-3}	7.49×10^{-6}
	TMGa, AsH_3	-2.26×10^{-1}	1.27×10^{-3}	3.18×10^{-6}
k_{12}^T[c]	H_2,SiH_4	-2.74×10^{-1}	-1.70	-6.35×10^{-3}
	N_2,SiH_4	-5.15×10^{-2}	-1.69	-4.94×10^{-3}
	H_2,N_2	-2.71×10^{-1}	-1.61	-9.15×10^{-3}
	TMGa, H_2	1.32	-1.54	-3.57×10^{-3}
	TMGa, N_2	6.36×10^{-1}	-1.58	-3.36×10^{-3}
	AsH_3,H2	8.86×10^{-1}	-1.57	-4.35×10^{-3}
	AsH_3, N2	3.09×10^{-1}	-1.55	-4.06×10^{-3}
	TMGa, AsH_3	1.94×10^{-1}	-1.79	-1.91×10^{-3}

[a] $\mu, k, c_p = c_0 + c_1 T + c_2 T^2$

[b] $D_{12} = D_{21} = \left(c_0 + c_1 T + c_2 T^2\right) / p$

[c] $k_{12}^T = -k_{12}^T = c_0 x_1 x_2 \left[1 + c_1 \exp(c_2 T)\right]$, for $x_1 \to 0$.

T is absolute temperature (K).

The collision integral Ω_μ in eq. (13) is a slowly-varying function of dimensionless temperature, $k_b T / \varepsilon$, and is tabulated in Table 3. k_b is the Boltzmann constant and ε is a characteristic energy of interaction between molecules which can be estimated by

$$\frac{\varepsilon}{k_b} = 0.77 T_c \tag{16}$$

or

$$\frac{\varepsilon}{k_b} = 1.15 T_b \tag{17}$$

where T_c and T_b are critical temperature and normal boiling point, respectively.

The thermal conductivity of the polyatomic gas is related to its viscosity by

$$k = \left(c_p + \frac{5}{4} R_g \right) \mu \tag{18}$$

where R_g is the gas constant.

Table 3 Dependence of collision integral Ω_μ on dimensional temperature $k_b T / \varepsilon$ (Bird *et al.*, 2002)

$k_b T/\varepsilon$	Ω_μ	$\Omega_{D,12}$	$k_b T/\varepsilon$	Ω_μ	$\Omega_{D,12}$	$k_b T/\varepsilon$	Ω_μ	$\Omega_{D,12}$
0.30	2.840	2.649	1.70	1.249	1.141	4.2	0.9598	0.8748
0.35	2.676	2.468	1.75	1.235	1.128	4.3	0.9551	0.8703
0.40	2.531	2.314	1.80	1.222	1.117	4.4	0.9506	0.8659
0.45	2.401	2.182	1.85	1.209	1.105	4.5	0.9462	0.8617
0.50	2.284	2.066	1.90	1.198	1.095	4.6	0.9420	0.8576
0.55	2.178.	1.965	1.95	1.186	1.085	4.7	0.9380	0.8537
0.60	2.084	1.877	2.00	1.176	1.075	4.8	0.9341	0.8499
0.65	1.999	1.799	2.10	1.156	1.058	4.9	0.9304	0.8463
0.70	1.922	1.729	220	1.138	1.042	5.0	0.9268	0.8428
0.75	1.853	1.667	2.30	1.122	1.027	6.0	0.8962	0.8129
0.80	1.790	1.612	2.40	1.107	1.013	7.0	0.8727	0.7898
0.85	1.734	1.562	2.50	1.0933	1.0006	8.0	0.8538	0.7711
0.90	1.682	1.517	2.60	1.0807	0.9890	9.0	0.8380	0.7555
0.95	1.636	1.477	2.7	1.0691	0.9782	10.0	0.8244	0.7422
1.00	1.593	1.440	2.8	1.0583	0.9682	12.0	0.8018	0.7202
1.05	1.554	1.406	2.9	1.0482	0.9588	14.0	0.7836	0.7025
1.10	1.518	1.375	3.0	1.0388	0.9500	16.0	0.7683	0.6878
1.15	1.485	1.347	3.1	1.0300	0.9418	18.0	0.7552	0.6751
1.20	1.455	1.320	3.2	1.0217	0.9340	20.0	0.7436	0.6640
1.25	1.427	1.296	3.3	1.0139	0.9267	25.0	0.7198	0.6414
1.30	1.401	1.274	3.4	1.0066	0.9197	30.0	0.7010	0.6235
1.35	1.377	1.253	3.5	0.9996	0.9131	35.0	0.6854	0.6088
1.40	1.355	1.234	3.6	0.9931	0.9068	40.0	0.6723	0.5964
1.45	1.334	1.216	3.7	0.9868	0.9008	50.0	0.6510	0.5763
1.50	1.315	1.199	3.8	0.9809	0.8952	75.0	0.6140	0.5415
1.55	1.297	1.183	3.9	0.9753	0.8897	100.0	0.5887	0.5180
1.60	1.280	1.168	4.0	0.9699	0.8845			
1.65	1.264	1.154	4.1	0.9647	0.8796			

For a mixture of different gases, as is usually the case in CVD processes, the viscosity and the thermal conductivity of the mixture are related to those of the individual components by

$$\mu = \sum_{i=1}^{N} \frac{x_i \mu_i}{\sum_{j=1}^{N} x_i \phi_{ij}} \tag{19}$$

$$k = \sum_{i=1}^{N} \frac{x_i k_i}{\sum_{j=1}^{N} x_i \phi_{ij}} \tag{20}$$

where

$$\phi_{ij} = \frac{1}{\sqrt{8}}\left(1+\frac{M_i}{M_j}\right)^{-1/2}\left[1+\left(\frac{\mu_i}{\mu_j}\right)^{1/2}\left(\frac{M_j}{M_i}\right)^{1/4}\right]^2 \tag{21}$$

The specific heat of the gaseous mixture is related to those of the individual components by

$$c_p = \sum_{i=1}^{N} x_i c_{p,i} \tag{22}$$

For applications that involve unknown mass diffusivity, it can be estimated by

$$D_{12} = 1.8583\times10^{-7}\frac{\sqrt{T^3\left(M_1^{-1}+M_2^{-1}\right)}}{p\sigma_{12}^2\Omega_{D,12}} \tag{23}$$

where the unit for pressure is atm and

$$\sigma_{12} = \frac{1}{2}\left(\sigma_1+\sigma_2\right) \tag{24}$$

$\Omega_{D,12}$ is a function of k_bT/ε_{12} that can be obtained from Table 7.3 using

$$\varepsilon_{12} = \sqrt{\varepsilon_1\varepsilon_2} \tag{25}$$

The concentration of the reactant is usually much lower than that of the carrier gas(es). When the reactant is a single gas diluted by the carrier gas, the diffusivity of the reactant to the carrier gaseous mixture is of interest. If the reactant is defined as component 1 in the precursor, and the carrier gases are components 2 through *N*, the diffusivity of the reactant – 1 – to the carrier gas mixture – *m* – can be obtained by

$$\frac{1-x_1}{D_{1m}} = \sum_{j=2}^{N}\frac{x_j}{D_{1j}} \tag{26}$$

4. THERMAL MODELING OF LCVD

4.1 Effects of Natural Convection

During LCVD, the spot on the substrate under laser irradiation is at a very high temperature (1200 K or higher). Temperature gradients in the source gases will cause natural convection in the chamber. The concentration of the gas mixture near the hot spot on the substrate is affected by the chemical reaction taking place on the substrate. Concentration differences in the chamber become another force driving natural convection in the chamber. For the case of LCVD by a stationary laser beam, Lee *et al.* (1995) concluded that the effect of natural convection on the thin film deposition rate was negligible and that the heat and mass transfer in the gases were dominated by diffusion. In the LCVD process, a laser beam scans the substrate and induces chemical reaction; the resulting product forms a line on the substrate. These lines, formed by multiple laser scans, are subsequently interwoven to form a part layer. To thoroughly understand the effects of various physical phenomena – including natural convection – on the LCVD process, natural convection during LCVD with a moving laser beam was investigated by Zhang (2003).

The physical model of LCVD under consideration is illustrated in Fig. 7. A substrate made of Incoloy 800 with a thickness of h is located in the bottom of a chamber. Before the vapor deposition starts, the chamber is evacuated and then filled with a mixture of H_2, N_2, and $TiCl_4$. A laser beam moves along the surface of the substrate with a constant velocity, u_b. The initial temperature of the substrate, T_i, is below the chemical reaction temperature. Vapor deposition starts when the surface temperature reaches the chemical reaction temperature. The chemical reaction that occurs on the top substrate surface absorbs part of the laser energy and consumes the $TiCl_4$. A concentration difference is thereby established and becomes the driving force for mass transfer. The physical model of the LCVD process includes: natural convection, heat transfer in the substrate and gases, and chemical reaction, as well as mass transfer in the gases.

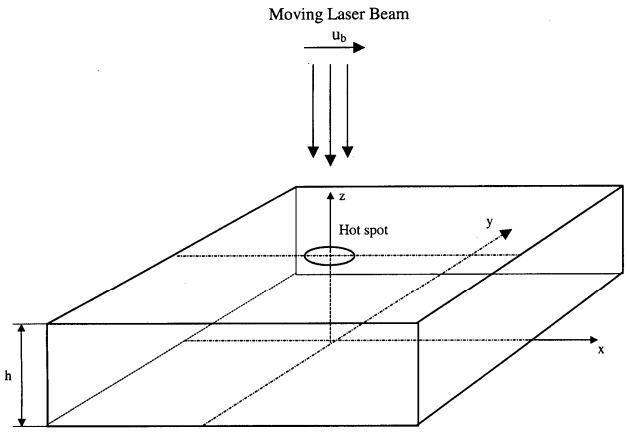

Figure 7 Physical model of Laser Chemical Vapor Deposition (Zhang, 2003)

The laser beam travels with a constant velocity u_b along the surface of the substrate, constituting a typical moving heat source problem. If the substrate is sufficiently large in comparison to the diameter of the laser beam, which has an order of magnitude of 10^{-3} m, a quasi-steady state occurs. The system appears to be in steady-state from the standpoint of an observer located in and traveling with the laser beam. By simulating LCVD with a moving laser beam in the moving coordinate system, the computational time will be substantially shortened, thereby enabling numerical simulation for a significant number of cases.

Heat transfer in the substrate and gases is modeled as one problem with different thermal properties in each region. In the substrate region, the velocity is set to zero in the numerical solution. The advantage of modeling the heat and mass transfer in the substrate and the gases as one problem is that the temperature distribution in the substrate and gases can be obtained by solving one equation. This eliminates the iteration procedure needed to match the boundary condition at the substrate-gas interface. Since the model geometry is symmetric about the xz plane, only half of the problem needs to be investigated. For a coordinate system moving with the laser beam, as shown in Fig. 7, the laser beam is stationary but the substrate and the chamber move with a velocity $-u_b$. The heat and mass transfer in the substrate and gases is governed by eqs. (2) – (5) and (7), with buoyancy forces due to temperature and concentration gradients accounted for,

but the Soret effect neglected (Zhang, 2003). For the substrate region, the thermal properties are those of Incoloy 800, the substrate material. For the gaseous region, the thermal properties are determined by the individual thermal properties of H_2, N_2, and $TiCl_4$ as well as their molar fractions [see eq. (19) – (20)]. The mass diffusivity of $TiCl_4$ in the gas mixture is determined by the Stefan-Maxwell equation, using the binary diffusivity of $TiCl_4$ with respect to all other species, which is calculated using the hard sphere model.

The heat flux at the substrate surface due to laser beam irradiation and chemical reaction is expressed as

$$q'' = \frac{2P\alpha_a}{\pi r_0^2}\exp\left[-\frac{2(x^2+y^2)}{r_0^2}\right] - \varepsilon\sigma(T^4 - T_\infty^4) + \rho_{TiN}\Delta H_R u_b \frac{d\delta}{dx}, \quad z = h \tag{27}$$

where ΔH_R is chemical reaction heat, and $d\delta/dt$ is the deposition rate. For a chemical reaction in the order of unity, the deposition rate is expressed as

$$\frac{d\delta}{dx} = -\frac{\gamma_{TiN}K_0}{u_b\rho_{TIN}}\exp\left(-\frac{E}{R_u T_s}\right)\omega_s \tag{28}$$

where ω_s represents the concentration of $TiCl_4$ at the surface of the substrate. The constant K_0 in eq. (28) is defined as $K_0 = (\omega_{H_2})_i(\omega_{N_2})_i^{1/2}K_0'$.

The coefficient γ_{TiN} in eq. (28) is a sticking coefficient defined as

$$\gamma_{TiN} = \begin{cases} 1 & T < T_m \\ 1 + (T_m - T_s)/(T_M - T) & T_m \le T \le T_M \\ 0 & T > T_M \end{cases} \tag{29}$$

where T_s is the surface temperature of the substrate, T_m is a threshold temperature below which the product of the chemical reaction can fully stick to the substrate, and T_M is another threshold temperature above which no product of chemical reaction can be stuck on the substrate. If the surface temperature is between T_m and T_M, the product of chemical reaction can only be partially stuck on the substrate. The values of T_m and T_M are chosen as 1473 K and 1640 K, respectively (Conde *et al.*, 1992a).

The boundary conditions of the velocities are

$$u = -u_b, \quad v = w = 0, \quad |x| \to \infty \tag{30}$$

$$v = \frac{\partial u}{\partial y} = \frac{\partial w}{\partial y} = 0, \quad y = 0 \tag{31}$$

$$u = -u_b, \quad v = w = 0, \quad y \to \infty \tag{32}$$

$$u = -u_b, \quad v = w = 0, \quad z = 0, \infty \tag{33}$$

The governing equations are discretized using the finite volume method (Patankar 1980); the SIMPLEC algorithm (Van Doormaal and Raithby, 1984) was employed to handle the linkage between velocity and pressure.

In order to verify the validity of the code, the calculation is initially made with conduction only in the substrate with a moving laser beam. The conduction problem in the substrate is achieved by setting the thermal conductivity of the gas to zero so that there is no heat conduction in the vapor phase. The steady state surface temperature obtained by numerical solution is compared with the temperature distribution caused by a moving point heat source. The temperature

expression of a semi-infinite body with a moving point heat source is (Carslaw and Jaeger, 1959)

$$T_s - T_i = \frac{P\alpha_a}{2\pi kr}\exp\left[-\frac{u(r+x)}{2\alpha}\right] \tag{34}$$

In order to simulate conduction in the substrate subject to a moving point heat source, the heat flux at the substrate surface due to laser beam irradiation is expressed as

$$q'' = \begin{cases} \dfrac{P\alpha_a}{\pi r_0^2} & r \le r_0 \\ 0 & r > r_0 \end{cases}, \quad z = h \tag{35}$$

where the moving heat source is assumed to be top-hat (uniform distribution) instead of a Gaussian distribution because the latter results in the energy spread in a large spot. Effects of surface radiation and chemical reaction on the surface heat flux are also neglected in eq. (35) in order to simulate pure conduction in the substrate.

The surface temperatures obtained by both methods are plotted in Fig. 2. The radius of the moving laser beam is r_0=1.41×10^{-4} mm, which is very small in order to simulate conduction in the substrate subject to a moving point heat source. It is seen that the overall agreement between the two solutions is very good except at the locations near x= 0. This discrepancy of the two results is due to the nature of the heat source modeled in the analytical and numerical solutions. The analytical result is for the temperature distribution caused by an infinitesimal heat source at x= 0, while the numerical temperature distribution result is for a finite size heat source. Considering the different models, the agreement between the numerical and analytical solutions is very good.

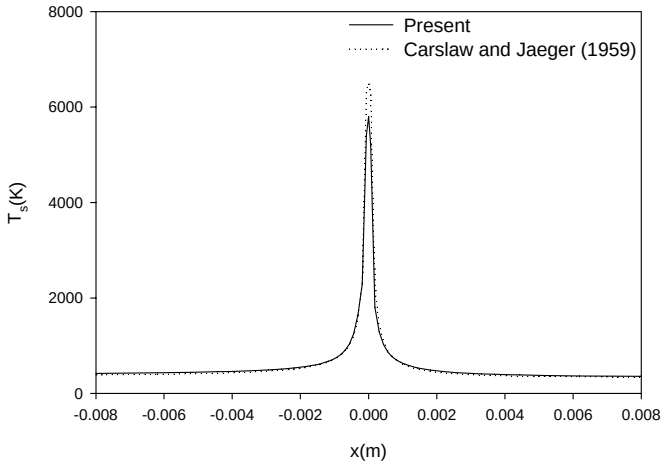

Figure 8 Comparison between analytical and numerical solutions for pure conduction

Numerical simulations of LCVD process are then performed with parameters similar to those in Conde *et al.* (1992a) and Zhang and Faghri (2000). The radius of the laser beam is very small compared with that of the chamber and therefore, the LCVD problem can be modeled as LCVD on a substrate with infinite length

and width. The validity of this assumption, of course, depends on the actual size of the substrate. On the other hand, it allows obtaining quasi-steady state solutions and conducting a parametric study. The computational domain (the size of the chamber) used in this paper is $0.5\times0.5\times0.125$ m³ ($x\times y\times z$) to ensure that the effect of the computational domain on the temperature distribution and deposited film can be eliminated. The thickness of the substrate is 5 mm and the bottom of the substrate is assumed to be adiabatic. The radius of the laser beam, which is defined as the radius where the laser intensity is $1/e^2$ of the intensity at the center of the laser beam, is 1.0×10^{-3} m. The absorptivity of the laser beam at the substrate surface is taken to be 0.23 (Conde et al., 1992a; Mazumder and Kar, 1995). The activation energy of the chemical reaction is taken to be E = 51.02 kJ/mol. The total pressure in the chamber is 207 torr and the partial pressure of titanium tetrachloride is 7 torr. The partial pressures of N_2 and H_2 are the same. The initial temperature of the substrate and gas is 338 K. The concentrations of different species can be obtained by using ideal gas law. With the conditions specified above, the constant K_0 in eq. (28) is 8.4m/s. Chemical reaction heat, ΔH_R, as determined by using JANAF thermochemical tables (Chase, 1986), is 5.379×10^6 J/kg.

Figure 3(a) and (b) shows the shape of the deposited TiN film obtained by using a scanning velocity of 1.2 mm/s and laser power of 300 W and 360W, respectively. The results show that the effect of natural convection on the shape of deposited film is negligible for the laser power of P = 300 W [see Fig. 9(a)]. When the laser power is increased to 360W, the effect of natural convection on the shape of the cross-section becomes important, although the cross sectional area is almost unchanged [see Fig. 9(b)]. A groove is observed on the top of the deposited film for P = 360 W due to a low sticking coefficient.

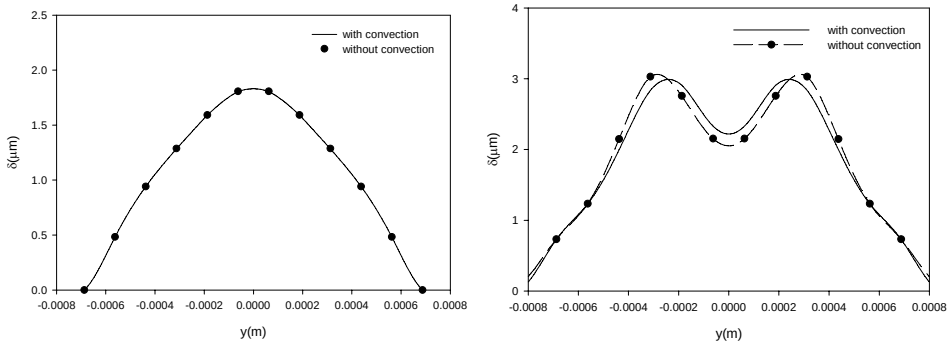

(a) P=300W, u_b=1.2mm/s (b) P=360W, u_b=1.2mm/s

Figure 9 Comparison of cross-sections (Zhang, 2003).

4.2 A Simulation-Based Correlation

It was demonstrated from the above results that the effect of natural convection on the shape of deposited film is negligible when the laser power is less than 360W. The shape of the cross-section of the film is slightly affected by

natural convection when the laser power is higher. However, the cross-sectional areas obtained by the models with and without natural convection are almost identical even for higher laser power. The numerical practices indicated that inclusion of natural convection would significantly increase the CPU time to obtain the converged solution, which would prevent a thorough parametric study. For the purpose of parametric study, the effect of natural convection can be neglected because it only has little effect on the shape of the deposited film and has no effect on the area of the cross-sectional area of the deposited film. Zhang (2004) carried out a thorough parametric study for LCVD with moving laser beams and a proposed a simulation-based correlation

The numerical simulations of the LCVD process are performed in a broader range. The total pressure in the chamber is 207 torr and the partial pressure of Titanium Chloride is maintained at 7 torr. The partial pressures of N_2 and H_2 are both maintained at 100 torr. The thickness of the substrate is 5 mm. The radius of the laser beam, which is defined as the radius where the laser intensity is $1/e^2$ of the intensity at the center of the laser beam, is 0.8 ~ 1.0 mm. The laser power varies from 180 to 360W and the scanning velocity ranged between 0.4 to 2 mm/s.

The effects of laser scanning velocity, laser power, and radius of the laser beam on the shapes of the deposited film were investigated. The results showed that a groove could be observed on the top of the film in conjunction with higher laser power and lower scanning velocity. The cross-sectional area, calculated by

$$A_c = \frac{2}{r_0^2}\int_0^\infty \delta dy \tag{36}$$

at different processing parameters, is shown in Fig. 10. It decreases with increasing scanning velocity. It also increases with increasing laser power and decreasing laser beam radius. In order to obtain a correlation for the dimensionless cross-sectional area, the results in Fig. 10 are replotted in Fig. 11. The dimensionless cross-sectional area is plotted as function of Biot number and Peclet number, which are defined by

$$\mathrm{Bi} = \frac{\alpha_a P}{\pi r_0 k_s (T_c - T_i)} \tag{37}$$

$$\mathrm{Pe} = \frac{u_b r_0}{\alpha_s} \tag{38}$$

where α_a is the absorptivity of the laser beam on the substrate surface, P is the laser power, r_0 is the radius of the laser beam, T_c is the chemical reaction temperature, T_i is the initial temperature of the gases, and u_b is the laser scanning velocity. The thermal conductivity k_s and the thermal diffusivity α_s in eqs. (37) – (38) are those of the substrate (Incoloy) at chemical reaction temperature.

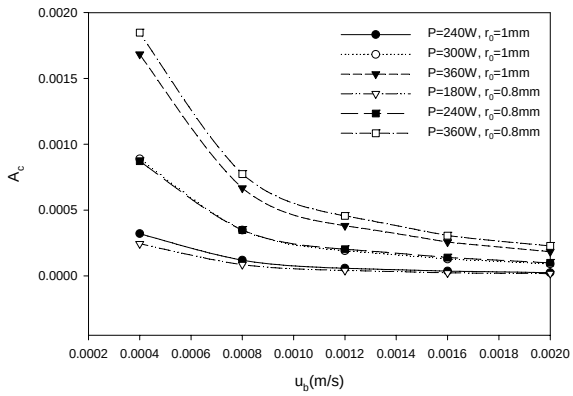

Figure 10 Dimensionless cross-sectional area vs. scanning velocity (Zhang, 2004).

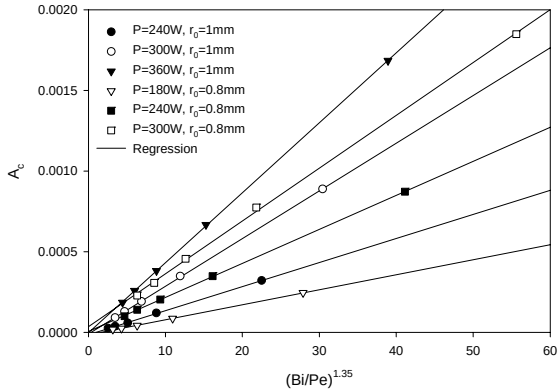

Figure 11 Dimensionless cross-sectional area vs. $(Bi/Pe)^{1.35}$ (Zhang, 2004).

It can be seen that the dimensionless cross-sectional areas are linear functions of $(Bi/Pe)^{1.35}$ for all cases. The dimensionless cross-sectional areas shown in Fig. 11 can be correlated into the following expression.

$$A_c = a_0 + a_1 \left(\frac{Bi}{Pe} \right)^{1.35} \tag{39}$$

where

$$a_0 = \begin{cases} -2.136\times10^{-5} + 6.126\times10^{-6}\,\mathrm{Bi} & r_0 = 1.0 \text{ mm} \\ -9.206\times10^{-5} + 9.352\times10^{-5}\,\mathrm{Bi} & r_0 = 0.8 \text{ mm} \end{cases} \tag{40}$$

$$a_1 = \begin{cases} 8.343\times10^{-7} + 1.423\times10^{-5}\,\mathrm{Bi} & r_0 = 1.0 \text{ mm} \\ -2.587\times10^{-5} + 4.372\times10^{-5}\,\mathrm{Bi} & r_0 = 0.8 \text{ mm} \end{cases} \tag{41}$$

The difference between the cross-sectional area obtained by numerical simulation and eq. (10) is less than 10%.

5. NON-EQUILIBRIUM HEAT TRANSFER IN PULSED LCVI

5.1 Introduction

Heat transfer in fluid-saturated porous media has been investigated extensively and excellent reviews are available in the literatures (Kaviany, 1995; Nield and Bejan, 1999). Nithiarasu *et al.* (1996) studied double-diffusive natural convection in an enclosure filled with fluid-saturated porous media using a generalized Non-Darcy approach and the non-Darcy effects on flow, heat, and mass transfer were investigated. Murphy *et al.* (1996) studied the effect of surface undulations on the natural convection heat transfer from an isothermal surface in a Darcian fluid-saturated porous enclosure using a finite element method. Khanafer and Chamkha (1998) numerically studied unsteady, laminar, 2-D hydromagnetic natural convection in an inclined square enclosure filled with fluid-saturated porous medium in presence of transverse magnetic field. The flow in the porous region is modeled using Brinkman-extended Darcy's law, which enabled non-slip condition at the walls. Effects of thermal stratification on double-diffusive natural convection in vertical porous square and wavy enclosures were studied by Kumar *et al.* (2002) and Kumar and Shalini (2003), respectively. While local thermal equilibrium between the porous matrix and the fluid is assumed in the above studies, it is well recognized that local equilibrium between different phases in a multiphase system cannot be achieved when thermal properties for different phases differ widely (Jiang *et al.*, 1999; Mohamad, 2000; Al-Amiri, 2002) or during rapid heating or cooling (Minkowycz *et al.*, 1999).

Since laser beam interacts with powder particle only and the precursors are assumed to be transparent during a LCVI process, heat transfer occurs in two steps: (1) absorption of laser beam by the powder particles, and (2) heat transfer from the powder particle to the precursors. If the laser-powder particle interaction time is much longer than the time that it takes for the powder particles and the gas to reach to thermal equilibrium, which is the case for continuous wave (CW) or long-pulsed laser, the local thermal equilibrium assumption between the powder and the gas is valid. Although CW laser is exclusively used in the existing LCVI experimental studies, the short-pulsed laser posses some advantages that are not available with continuous laser. One advantage is that the porosity of the final product can be controlled by controlling the degree of LCVD on the powder particle surface via adjustment of pulse width and repetition rate. Other advantages include achieving LCVD at a much lower average laser power, more accurate control of the dimension of the final product, etc. Since the thermal physical property of the precursors and the particles differ significantly and LCVI with short-pulsed laser is a rapid process, the powder particles and precursors may not be able to reach local equilibrium and consequently, a non-equilibrium model for transport phenomena in the precursors and particles must be developed. In order to explore LCVI with short-pulsed laser, non-equilibrium phenomenon in a powder layer subject to short-pulsed volumetric heat source was investigated in by Zhang (2006).

5.2 Nonequilibrium Heat Transfer Model

The physical model of the problem under consideration is shown in Fig. 12. A powder layer with a thickness of L and an initial temperature of T_i is subjected to a temporal Gaussian heat source with a FWHM (Full Width at Half Maximum) pulse width of t_p and fluence of J (J/m^2). Since the powder layer is porous, the heat source can penetrate the powder layer and the thermal energy is absorbed within the powder layer, not only at the surface of the powder layer. It is assumed that heat transfer is 1-D along the thickness of the powder layer only. The effect of chemical reaction heat on the heat transfer in the powder layer is neglected because its effect on the deposition rate was negligible as shown by Zhang and Faghri (2000). The porosity of the powder layer during irradiation of one single pulse is assumed to be constant because the amount of deposition in the duration of one short pulse is very small. The effect of convection in the gas phase is also neglected because the laser pulse is very short. Therefore, the problem under consideration becomes heat conduction in a gas-saturated powder layer with internal heat source.

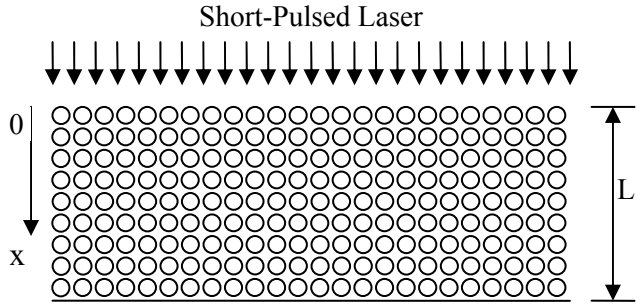

Figure 12 Nonequilibrium heat conduction in powder layer (Zhang, 2006)

Since the precursors and the particles are not in thermal equilibrium, a two-energy equation model will be employed to describe heat transfer in precursors and particles. The energy equations of the powder particles (s) and the precursors (g) can be respectively expressed as

$$(1-\varphi)(\rho c_p)_s \frac{\partial T_s}{\partial t} = \frac{\partial}{\partial x}\left[k_{s,eff} \frac{\partial T_s}{\partial x} \right] + \dot{q}_s''' - G(T_s - T_g) \tag{42}$$

$$\varphi(\rho c_p)_g \frac{\partial T_g}{\partial t} = \frac{\partial}{\partial x}\left[k_{g,eff} \frac{\partial T_g}{\partial x} \right] + G(T_s - T_g) \tag{43}$$

where $k_{s,eff}$ and $k_{g,eff}$ are the effective thermal conductivities of the solid and gas phases, respectively. During the LCVI process, the powder particles are partially joined together and therefore, it can be assumed that heat conductions occurred in both phases are in parallel. The effective thermal conductivity for solid and gas phases are $k_{s,eff} = (1-\varphi)k_s$ and $k_{g,eff} = \varphi k_g$, respectively. Similar assumptions can be found in existing non-equilibrium models for fluid-saturated porous media (e.g., Al-Amiri, 2002).

The internal heat source term in eq. (42) is

$$q_s''' = 0.94\frac{1-R}{t_p\delta}J\exp\left[-\frac{x}{\delta}-2.77\left(\frac{t}{t_p}\right)^2\right] \tag{44}$$

where R is reflectivity, and δ is the optical penetration depth. In arrival of eq. (44), the time t =0 is defined as the time when the peak of the heat source occurs. For spherical particle, the coupling coefficient between powder particle and the gas is determined by

$$G = \frac{6(1-\varphi)h_p}{d_p} \tag{45}$$

where d_p is the diameter of the powder particle, h_p is the heat transfer coefficient at the particle surface. Mohamad (2000) suggested that heat transfer between the powder particles and the fluid can be estimated by using the empirical correlation for natural convection from an isolated sphere (Churchill, 1983):

$$\mathrm{Nu} = \frac{h_p d_p}{k_g} = 2 + 0.589\frac{\mathrm{Ra}_d^{1/4}}{[1+(0.496/\mathrm{Pr})^{9/16}]^{4/9}} \tag{46}$$

In absence of natural convection in the gas phase, the Nusselt number based on the particle diameter is

$$\mathrm{Nu} = \frac{h_p d_p}{k_g} = 2 \tag{47}$$

The initial conditions of the problem are

$$T_s(x,-\infty) = T_g(x,-\infty) = T_i \tag{48}$$

The surface of the powder layer subjected to heating is also subject to convective cooling, i.e.,

$$-k_{s,eff}\left.\frac{\partial T_s}{\partial x}\right|_{x=0} = h_0(T_s - T_\infty)\,,\quad -k_{g,eff}\left.\frac{\partial T_g}{\partial x}\right|_{x=0} = h_0(T_g - T_\infty) \tag{49}$$

while the bottom of the powder layer is adiabatic

$$\left.\frac{\partial T_g}{\partial x}\right|_{x=L} = \left.\frac{\partial T_s}{\partial x}\right|_{x=L} = 0 \tag{50}$$

The heat transfer during laser-powder layer interaction can be solved by using finite different method (Patankar, 1980). Equations (42) and (43) are discretized using an implicit scheme and the resulting algebraic equations are solved using Tri-Diagonal Matrix Algorithm (TDMA). Heat transfer in powder and gas are coupled and therefore iteration is needed. After the grid number independent test, the grid number for all computations is 502. Numerical solution is started from $t = -5t_p$ with a time step of $\Delta t = t_p/100$ until $t = 5t_p$. The time step is changed to $\Delta t = t_p$ for $t > 5t_p$ and again to $\Delta t = 100t_p$ after $t = 100t_p$. The numerical solution for each time step begins with solution of the powder temperature, T_s, from eq. (42) based on an assumed gas temperature distribution, T_g . The powder temperature is then used to obtain the updated gas temperature T_g^{new} from eq. (43), which is then compared with the assumed gas temperature, T_g . If the maximum

difference between T_g^{new} and T_g is less than a small tolerance value, 10^{-6}K, end the iteration for the current time step and go to the next time step. Otherwise, update T_g and repeat the iteration until the convergence criterion is met. Underrelaxation is not necessary during the iteration.

5.3 Effects of Pulse Duration on Nonequilibrium Heat Transfer

Numerical simulations are performed for a system with silicon carbide powder and tetramethylsilane (TMS) gas (Dai *et al.* 2003). The thermal physical properties of the silicon carbide are $\rho_s = 3.21\times10^3 \text{kg/m}^3$, $c_{ps} = 660\text{J/kg-K}$, $k_s = 58.86\text{W/m-K}$. The porosity of the powder layer is set as 0.42, which is within the range of randomly packed powder bed (Kaviany, 1995). The specific heat of the TMS as obtained from JANAF Thermochemical Tables (Chase, 1986) is $c_{pg} = 3438\text{J/kg-K}$. The thermal conductivity of TMS is $k_g = 0.536\text{W/m-K}$, which is derived by using the method in Bird *et al.* (2002) at 1273K. The density of the TMS is $\rho_g = 0.045\text{kg/m}^3$, which is obtained using ideal gas law with a pressure of 10 torr (Dai *et al.* 2003). The reflectivity of the laser beam is taken as $R = 0.6$. The initial temperature of the powder layer for all cases discussed below is $T_i = 300$ K . The optical penetration depth is related to the powder particle size, porosity, and the absorptivity of the powder material. Alexandre *et al.* (2004) measured the optical penetration depth of the silicon carbide powder under irradiation of Nd:YAG laser and found that the penetration depth is about 1.5 to 2 times of the particle diameter. The optical penetration depth in eq. (44) is therefore, taken as $\delta = 2d_p$ in this paper. The particle sizes to be studied in this paper are d_p = 15, 20 and 25 μm , which are consistent with the particle size used in the LCVI experiments (Crocker *et al.*, 2002; Dai *et al.* 2003).

The effect of pulse width on the maximum powder temperature and the maximum temperature differences is shown in Fig. 13. The amount of laser energy delivered to the powder layer is the same for all cases because the laser fluence is kept at $J = 1.25\times10^5 \text{J/m}^2$. It can be seen that the powder temperature at the heating surface decreases with increasing powder particle diameter because the optical penetration depth increases with increasing powder particle diameter. The powder temperature at the heating surface decreases with increasing pulse width because the same laser energy spread over a longer period of time for larger pulse width. When the laser pulse width is shorter than 10 ns, the maximum temperature difference between the powder particle and gas decreases with increasing powder particle size. The effect of particle diameter on the maximum temperature difference becomes weaker with increase pulse width. After the laser pulse length is longer than 10 ns, the maximum temperature difference decreases with decreasing powder particle but the effect of particle size is very insignificant. When the laser pulse width is longer than 100ns, the effect of particle diameter is almost vanished. For all particle sizes studied in Fig. 13, the maximum temperature difference decreases with increase pulse width. After the laser pulse width is longer than 1 μs , the non-equilibrium phenomenon becomes very

insignificant and the laser-powder interaction can be modeled using equilibrium model.

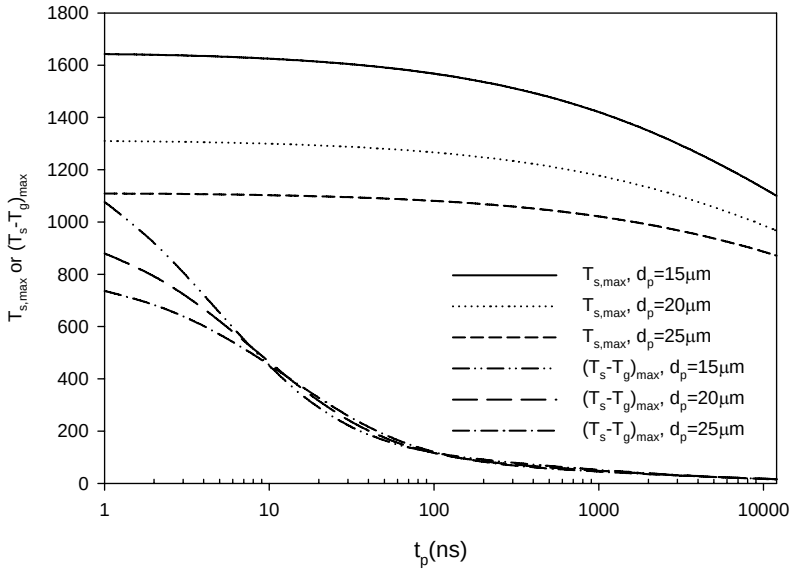

Figure 13 Maximum powder temperature and maximum temperature difference vs. pulse width ($J = 1.25 \times 10^5 \text{ J/m}^2$; Zhang, 2006)

6 CONCLUSIONS

Advances in thermal modeling of laser chemical vapor deposition and infiltration are reviewed in this chapter. In contrast to conventional CVD, in which the entire susceptor is heated, only a very small spot on the substrate is heated by a directed laser beam during LCVD. The mechanism to bound powder particles together in a LCVI process is vapor deposition of solid material on the powder particle surface by decomposition of gas precursors. Extensive experimental works about LCVD/LCVI have been carried out and various applications of these new techniques have been discovered. The inherent nature of LCVD/LCVI makes them very ideal to fabricate ceramics and metal parts that are either impossible or very difficult to be manufactured by any other methods. Accurate prediction and control LCVD/LCVI require a model of the processes that incorporate heat/mass transfer, chemical reaction kinetics, and chemical thermodynamics. Kinetic data that are important to modeling LCVD/LCVI are difficult to obtain and are currently compiled for only a limited number of chemical systems. Thermodynamic modeling is very useful for precursor selection; however, it cannot predict the deposition rate that is very critical for design of LCVD/LCVI systems. The generalized governing equations for transport phenomena and chemical reaction during LCVD as well as transport properties of the gaseous precursors are presented.

Natural convection in the LCVD of TiN films on a substrate with a moving laser beam was investigated numerically. The results show that the effect of natural convection on the shape of deposited films is negligible for a laser power

of 300 W. When the laser power is increased to 360 W, a groove is observed on top of the thin film and the effect of natural convection on the shape of the cross sectional area becomes important. A parametric study on the LCVD of TiN film on a substrate with moving laser beam is presented. The results showed that a groove could be observed on the top of the film for higher laser power and lower scanning velocity. The cross-sectional area decreases with increasing scanning velocity. It also increases with increasing laser power and decreasing laser beam radius. A simulation-based correlation on the dimensionless cross-sectional area is obtained.

Heat transfer in a thin powder layer subject to a short-pulsed volumetric heat source is modeled using a non-equilibrium model. The degree of non-equilibrium in the process, as measured using the maximum temperature difference between powder and gas, decreases with increase laser pulse width and it becomes insignificant for the laser pulse longer than $1\,\mu s$. The peak temperature and the maximum temperature difference between powder and gas increase with increasing powder particle diameter. The times at which peak temperatures and maximum temperature difference occur are not affected by increasing laser fluence, but the maximum temperatures and the maximum temperature difference between the powder and gas increase significantly with increasing laser fluence.

ACKNOWLEDGEMENT

The work presented in this chapter is supported in part by the US National Science Foundation under grant number CBET -0730143.

NOMENCLATURE

a_{ij}	stoichiometric coefficient for the i^{th} component in the j^{th} chemical reaction
C	concentration (kg/m³)
c_p	specific heat (J/kgK)
D	mass diffussivity (m²/s)
$\mathbf{D}$	strain tensor
d_p	diameter of the powder particle [m]
E	activation energy (kJ/mol)
G	coupling coefficient [W/m^3-K]
h	thickness of the substrate (m)
h_0	heat transfer coefficient at the powder bed surface [W/m^2-K]
h_p	heat transfer coefficient at the powder particle surface [W/m^2-K]
$\mathbf{I}$	unit tensor
$\mathbf{J}$	mass flux vector due to ordinary diffusion (kg/m^2-s)
J	heat source fluence (J/m^2)
k	thermal conductivity (W/mK)
K_0'	Arrhenius constant
L	thickness of the powder layer
M	molecular weight (g/mol)
Nu	Nusselt number

$\dot{m}''$ mass flux (kg/m²)
n_r number of reactants
n_p number of gaseous products
P laser power (W)
p pressure (Pa)
q'' heat flux (W/m²)
q_s''' intensity of the internal heat source [W/m^3]
r_o radius of the laser beam (m)
R_u universal gas constant (=8.314kJ/kmol)
S source term in the energy equation
S_c source term in the mass transfer equation
t time (s)
t_p HWHM (Half Width at Half Maximum) pulse width [s]
T temperature (K)
u velocity component in x direction (m/s)
v velocity component in y direction (m/s)
V velocity vector (m/s)
w velocity component in z direction (m/s)
x coordinate in length direction(m)
y coordinate in width direction (m)
z coordinate in height direction (m)

Greek Symbols

α diffusivity (m²/s)
α_a absorptivity
β coefficients of thermal expansion (1/K)
β_c concentration expansion coefficients (m³/kg)
γ sticking coefficient
φ porosity
δ thickness of the deposited film (m), or optical penetration depth of the powder layer (m)
ΔH_R heat of chemical reaction (J/kg)
ε emissivity
ρ density (kg/m³)
σ collision diameter (Å)
$\boldsymbol{\tau}'$ stress tensor (N/m^2)

Subscripts

g gas
i initial value
s substrate, or solid
∞ infinite

REFERENCES

Al-Amiri, A.M., 2002, "Natural Convection in Porous Enclosures: The Application of the Two-Energy Equation Model," *Numerical Heat Transfer*, Part A., Vol. 41, pp. 817-834.

Alexandre, T., Giovanola, J., Vaucher, S., Beffort, O., Vogt, U., 2004, "Layered Manufacturing of Porous Ceramic Parts from SiC Powders and Preceramic Polymers," *Proceedings of the 4th Laser Assisted Net Shape Engineering (LANE)*, Erlangen, Germany, pp. 497-505.

Bird, R.B., Stewart, W.E., and Lightfoot, E.N., 2002, *Transport Phenomena*, 2nd ed., John Wiley and Sons, New York.

Birmingham, B.R. and Marcus, H.L., 1994, "Silicon Carbide Shaped by Selective Area Laser Deposition Vapor Infiltration," *Proc. of the 5th Solid Freeform Fabrication Symposium*, Austin, TX, pp. 348-355.

Carslaw, H.S., and Jaeger, J.C., 1959, *Conduction of Heat in Solids*, Clarendon, Oxford.

Chase, W.M., 1986, JANAF Thermochemical Tables, 3rd Edition, *J. Phys. Chem. Ref. Data*, Vol. 14, Suppl. 1.

Churchill, S.W., 1983, "Free Convection Around Immersed Bodies," *Heat Transfer Design Handbook*, Schlunder, E.U. Ed., Hemisphere, New York, NY.

Conde, O., Kar, A., and Mazumder, J., 1992a, "Laser Chemical Vapor Deposition of TiN Dot: A Comparison of Theoretical and Experimental Results," *J. Applied Physics,* Vol. 72, pp. 754-761.

Conde, O., Ferreira, M.L.G., and Hochholdinger, P., and Silvestre, A.J., 1992b, "CO_2 laser induced CVD of TiN," Applied Surface Science, Vol. 54, pp. 130-134.

Crocker, J.E., Sun, L, Shaw, L.L., and Marcus, H.L., 1998, "Preparation and Properties of In-Situ Device Using the SALD and SALDVI techniques," *Proceedings of the 9th Solid Freeform Fabrication Symposium*, pp. 543-547.

Crocker, J.E., Shaw, L.L., and Marcus, H.L., 2000, "Gas-Phase Solid Freeform Fabrication of SALDVI of SiC Cermets," *Mat. Res. Soc. Proc., Vol. 625, pp. 211-215.*

Crocker, J.E., Wei, H., Shaw, L.L., and Marcus, H.L., 2001, "SALDVI of SiC into Metal and Ceramic Powders," *Proceedings of the 12th Solid Freeform Fabrication Symposium*, pp. 163-169.

Crocker, J.E., Shaw, L.L., and Marcus, H.L., 2002, "Powder Effects in SiC Matrix Layered Structures Fabricated Using Selective Area Laser Deposition Vapor Infiltration," *J. Materials Science*, Vol. 37, pp. 3149-3154.

Dai, K., Crocker, J., Shaw, L., and Marcus, H., 2000, "Finite Element Analysis of the SALDVI Process," *Proceedings of the 11th Solid Freeform Fabrication Symposium*, pp. 393-398.

Dai, K., Crocker, J., Shaw, L., and Marcus, H., 2001, "Modeling of Selective Area Laser Deposition Vapor Infiltration (SALDVI) of Silicon Carbide," *Proceeding of the 13th Solid Freeform Fabrication Symposium*, pp. 392-399.

Dai, K., Crocker, J., Shaw, L., and Marcus, H., 2003, "Thermal Modeling of Selective Area Laser Deposition (SALD) and SALD Vapor Infiltration of Silicon Carbide," *Rapid Prototyping Journal,* Vol. 9, pp. 231-239.

Elyukhin, V.A., Garcia-Salgado, G., and Pena-Sierra, R., 2002, "Thermodynamic Model for Low Temperature Metalorganic Chemical Vapor Deposition of GaN," *Journal of Applied Physics*, Vol. 91, pp. 9091-9094.

Faghri, A., and Zhang, Y., 2006, *Transport Phenomena in Multiphase Systems*, Elsevier, Burlington, MA.

Figueras, A., Garelik, S., and Rodroguez-Clememe, R. 1991a, "A morphological and Structural Study *of* SiC layers obtained by LPCVD using Tetramethylsilane," *Journal of Crystal Growth*, Vol. 100, pp. 528.

Figueras, A., Garelik, S., Santiso, J., and Rodrogucz-Clemente, R., Annas, B., Combescure, C. Berjoan, R., Saurel, J. M., and Caplain, R., 1991b, "Growth and Propcnics of CVD-SiC layers obtained by LPCVD using Tetramcthylsilane," *Journal of Materials Science*. Vol. 23, pp. 1632.

Figueras, A., Garelik, S., Santiso, J., and Rodrogucz- Clemente, R., 1992, "Growth and Properties of CVD-SiC layers using Tetramethylsilanc," *Material Science and Engineering*, B11, pp. 83.

Gordon, S., and McBride, B.J., 1976, Computer Program for Calculation of Complex Chemical Equilibrium Compositions, Rocket Performance, Incident and Reflected Shocks and Chapman-Jouguet Detonations, NASA Lewis Research Center, NASA SP-273, March, 1976.

Han, J., and Jensen, K.F., 1994, "Combined Experimental and Modeling Studies of Laser-assisted Chemical Vapordeposition of Copper from Copper(I)-hexafluoroacetylacetonate Trimethylvinylsilane," *J. Applied Physics*, Vol. 75, pp. 2240-2250.

Herring, R.B., 1990, "Silicon Epitaxy," In *Handbook of Semiconductor Silicon Technology*, edited by O'Mara, W.C., Herring, R.B., and Hunt, L.P., Noyes Publications, Park Ridge, NJ, pp. 258-336.

Jakubenas, K.J., Birmingham, B., Harrison, S., Crocker, J., Shaarawi, M.S., Tompkins, J.V., Sanchez, J., and Marcus, H.L., 1997, "Recent Development in SALD and SALDVI," *Proceedings of 7th International Conference on Rapid Prototyping*, San Francisco, CA.

Jakubenas, K.J., Sanchez, J.M., and Marcus, H.L., 1998, "Multiple Material Solid Free-form Fabrication by Selective Area Laser Deposition," *Materials and Design*, Vol. 19, pp. 11-18.

Jacquot, Y., Zong, G.S., and Marcus, H.L., 1995, "Modeling of Selective Laser Deposition for Solid Freeform Fabrication," *Proceedings of Solid Freeform Fabrication Symposium 1995*, pp. 74-82.

Jean, D.L., Duty, C.E., Fuhrman, B.T., and Lackley, W.J., 1999, "Precision LCVD System Design with Real Time Process Control," *Proceedings of 10th Solid Freeform Fabrication Symposium*, pp. 59-65.

Jean, D.L., Duty, C.E., Fuhrman, B.T., and Lackley, W.J., 2000, "Precision Carbon Deposition Using Pyrolytic Laser Chemical Vapor Deposition," *Proceedings of 11th Solid Freeform Fabrication Symposium*, pp. 73-79.

Jiang, P.X., Ren, Z. P., and Wang, B.X., 1999, "Numerical Simulation of Forced Convection Heat Transfer in Porous Plate Channels Using Thermal Equilibrium and Nonthermal Equilibrium Models," *Numerical Heat Transfer,* Part A, Vol. 35, pp. 99-113.

Kar, A., and Mazumder, J., 1989, "Three-Dimensional Transient Thermal Analysis for Laser Chemical Vapor Deposition on Uniformly Moving Finite Slabs," *J. of Applied Physics*, Vol. 65, pp. 2923-2934.

Kar, A., Azer, M.N., and Mazumder, J., 1991, "Three- Dimensional Transient Mass Transfer Model for Laser Chemical Vapor Deposition of Titanium on Stationary Finite Slabs," *J. of Applied Physics* Vol. 69, pp. 757-766.

Kaviany, M., 1995, *Principles of Heat Transfer in Porous Media*, 2nd Edition, SpringerVerlag, New York.

Khanafer, K.M, and Chamkha, A. J., 1998, "Hydromagnetic Natural Convection from an Inclined Porous Square Enclosure with Heat Generation," *Numerical Heat Transfer,* Part A, Vol. 33, pp. 891-910.

Kumar, B.V.R., Singh, P., and Bansod, V.J., 2002, "Effect of Thermal Stratification on Double-Diffusive Natural Convection in a Vertical Porous Enclosure," *Numerical Heat Transfer,* Part A, Vol. 41, pp. 421-447.

Kumar, B.V.R., and Shalini, 2003, "Natural Convection in a Thermally Stratified Wavy Vertical Porous Enclosure," *Numerical Heat Transfer,* Part A, Vol. 43, pp. 753-776.

Lee, Y.L., Tompkins, J.V., Sanchez, J.M. and Marcus, H.L., 1995, "Deposition Rate of Silicon Carbide by Selected Area Laser Deposition," *Proceedings of Solid Freeform Fabrication Symposium 1995*, pp. 433-439.

Mahajan, R.L., 1996, "Transport Phenomena in Chemical Vapor-Deposition Systems," *Advances in Heat Transfer*, Academic Press, San Diego, 1996.

Marcus, H.L, Zong, G., and Subramanian, P.K., 1993, "Residual Stresses in Laser Processed Solid Freeform Fabrication, Residual Stresses in Composites," *Measurement, Modeling and Effect on Thermomechanical Properties*, Barrera, E.V. and Dutta, I., eds., TMS, pp. 257-271.

Maxwell, J., Krishnan, R., and Haridas, S., 1997, "High Pressure, Convectively-Ehhanced Laser Chemical Vapor Deposition of Titanium," *Proceedings of Solid Freeform Fabrication Symposium 1997*, pp. 497-504.

Maxwell, J., Larsson, K., Boman, M., Hooge, P., Willaims, K., and Coane, P., 1998a, "Rapid Prototyping of Functional Three-Dimensional Microsolenoids and Electromagnets by High-Pressure Laser Chemical Vapor Deposition," *Proceedings of Solid Freeform Fabrication Symposium 1998*, pp. 529-536.

Maxwell, J., Shah, J., Webster, T., and Mock, J., 1998b, "Rapid Prototyping of Titanium Nitride Using Three-Dimensional Laser Chemical Vapor Deposition," *Proceedings of Solid Freeform Fabrication Symposium 1998*, pp. 575-580.

Maxwell, J, Boman, M., Williams, K., Larsson, K. , Jaikumar, N., and Saiprasanna, G., 1999 "High-Speed Laser Chemical Vapor Deposition of. Amorphous Carbon Fibers, Stacked Conductive Coils, and Folded Helical Springs," *Part of the SPIE Conference on Micromachining and Microfabrication Process Technology V, SPIE* vol. 3874, Santa Clara, CA.

Mazumder, J., and Kar, A., 1995, Th*eory and Application of Laser Chemical Vapor Deposition*, Plenum Publishing Co., New York, NY.

Minkowycz, W. J., Haji-Sheikh, A., and Vafai, K., 1999, "On Departure from Local Thermal Equilibrium in Porous Media due to a Rapidly Changing Heat Source: the Sparrow Number," *International Journal of Heat and Mass Transfer*, Vol. 42, pp. 3373-3385.

Mohamad, A.A., 2000, "Nonequilibrium Natural Convection in a Differentially Heated Cavity Filled with a Saturated Porous Matrix," ASME *J. Heat Transfer*, Vol. 122, pp. 380-384.

Murphy, P.V.S.N., Kumar, B.V.R., and Singh, P., 1996, "Natural Convection Heat Transfer from a Horizontal Wavy Surface in a Porous Enclosure," *Numerical Heat Transfer,* Part A, Vol. 31, pp. 207-221.

Nield, D.A., and Bejan, A., 1999, *Convection in Porous Media*, 2nd ed., Springger-Verlag, New York.

Nithiarasu, P., Seetharamu, K. N., and Sundararaian, L, 1996, "Double-Diffusive Natural Convection in an Enclosure Filled with Fluid-Saturated Porous Medium: A Generalized Non-Darcy Approach," *Numerical Heat Transfer,* Part A, Vol. 30, pp. 413-426.

Patankar, S.V., 1980, *Numerical Heat Transfer and Fluid Flow*, Hemisphere, Washington, DC.

Powell, C., Blocher, M., and Oxley, J., 1966, *Vapor Deposition*, John Wiley and Sons, New York.

Shaarawi, M.S., Sanchez, J.M., Kan, H., and Manthiram, A., 2000, "Modeling of Laser-Induced Chemical Vapor Deposition of Silicon Carbide Rids from Tetramethylsilane," J. Am. Ceram. Soc., Vol. 83, pp. 1947-1952.

Sivaram, S., 1995, *Chemical Vapor Deposition:* Th*ermal and Plasma Deposition of Electronic Materials*, Kluwer Academic Publishers, Bordrecht, Netherlands.

Sun, L., Jakubenas, K.J., Crocker, J.E., Harrison, S., Shaw, L.L., and Marcus, H.L. 1998a, "In Situ Thermocouples in Micro-Components Fabricated Using SALD/SALDVI Techniques: I Thermochemical Modeling," *Materials and Manufacturing Processes*, Vol. 13, pp. 859-882.

Sun, L., Jakubenas, K.J., Crocker, J.E., Harrison, S., Shaw, L.L., and Marcus, H.L. 1998b, "In Situ Thermocouples in Micro-Components Fabricated Using SALD/SALDVI Techniques: II Evaluation of Processing Parameters," *Materials and Manufacturing Processes*, Vol. 13, pp. 883-907.

Sun, L., Jakubenas, K.J., Crocker, J.E., Harrison, S., Shaw, L.L., and Marcus, H.L. 1998c, "In Situ Thermocouples in Micro-Components Fabricated Using SALD/SALDVI Techniques: III Fabrication and Properties of the SiC/C Thermocouple Device," *Materials and Manufacturing Processes*, Vol. 13, pp. 909-919.

Taylor, C.A., Wayne, M.F., and Chiu, W.K.S., 2004, "Microstructural Characterization of Thin Carbon Films Deposited from Hydrocarbon Mixtures," *Surface and Coatings Technology,* Vol. 182, pp. 131-137.

Ueda, O., 1996, *Reliability and Degradation of III-V Optical Devices*, Artech House, Inc., Boston.

Van Doormaal, J.P., and Raithby, G.D., 1984, "Enhancements of the Simple Method for Predicting Incompressible Fluid Flows," *Numerical Heat Transfer*, Vol. **7**, pp. 147-163.

Williams, K., Maxwell, J., Larsson, K., and Boman, M., 1999, "Freeform Fabrication of Functional Microsolenoids, Electromagnets and Helical Springs Using High-Pressure Laser Chemical Vapor Deposition," *Proceedings of the* 1999 *12th IEEE International Conference on Micro Electro Mechanical Systems! MEMS,* pp. 232-237.

Zhang, Y., 2003, "Quasi-Steady State Natural Convection in Laser Chemical Vapor Deposition using a Moving Laser Beam," ASME *J. Heat Transfer*, Vol. 125, No. 3, pp. 429-437.

Zhang, Y., 2004a, "Effect of Natural Convection on Laser Chemical Vapor Deposition with a Stationary Laser Beam," *Int. J. Heat and Fluid Flow*, Vol. 25, No. 4, pp. 683-691.

Zhang, Y., 2004b, "A Parametric Study on Shape and Cross-Sectional Area of the Thin Film Produced by Laser Chemical Vapor Deposition with a Moving Laser Beam," ASME *J. Manufacturing Science and Engineering,* Vol. 126, No. 4, pp. 796-800.

Zhang, Y., and Faghri, A., 2000, "Thermal Modeling of Selective Area Laser Deposition of Titanium Nitride on a Finite Slab with Stationary and Moving Laser Beams," *Int. J. Heat Mass Transfer*, Vol. 43, pp. 3835-3846